Inorg. Chem. **2008**, *47*, 1107–1119

Synthesis, Structure, and Physicochemical Properties of Dinuclear Ni^{II} Complexes as Highly Efficient Functional Models of Phosphohydrolases

Alessandra Greatti,[†] Marciela Scarpellini,[†,‡] Rosely A. Peralta,[†] Annelise Casellato,[†] Adailton J. Bortoluzzi,[†] Fernanado R. Xavier,[†] Rafael Jovito,[†] Marcos Aires de Brito,*[,†] Bruno Szpoganicz,[§] Zbigniew Tomkowicz,[||,⊥] Michal Rams,[⊥] Wolfgang Haase,[||] and Ademir Neves*[,†]

Laboratório de Bioinorgânica e Cristalografia (LABINC) and Laboratório de Equilíbrio Químico, Departamento de Química, Universidade Federal de Santa Catarina, 88040-900 Florianópolis, Santa Catarina, Brazil, Institut für Physikalishe Chemie, Technische Universität Darmstadt, Petersenstrasse 20, D-64287-Darmstadt, Germany, and Institute of Physics, Reymonta 4, Jagiellonian University, PL-30-059 Krakow, Poland

Received October 29, 2007

As metal ions are present in the catalytic sites of several enzymes, attention has been focused on the synthesis and characterization of metal complexes able to act as biomimetic functional and structural models for these systems. In this study, a novel dinuclear Ni^{II} complex was synthesized, $[Ni_2(L2)(OAc)_2(CH_3CN)]BPh_4$ (**2**) (HL2 = 2-[*N*-(2-(pyridyl-2-yl)ethyl)(1-methylimidazol-2-yl)amin omethyl]-4-methyl-6-[*N*-(2-(imidazol-4-yl)ethyl)amino methyl]phenol), employing a new unsymmetrical dinucleating ligand containing N,O-donor groups as a model for hydrolases. Complex **2** was characterized by a variety of techniques including: elemental analysis, infrared and UV–vis spectroscopies, molar conductivity, electrochemistry, potentiometric titration, magnetochemistry, and single-crystal X-ray diffractometry. The structural and magnetochemical data of **2** allow us to consider this complex as a structural model for the active site of the ureases, as previously reported for $[Ni_2(L1)(OAc)_2(H_2O)]ClO_4 \cdot H_2O$ (**1**) (HL1 = 2-[*N*-bis-(2-pyridylmethyl)aminomethyl]-4-methyl-6-[*N*-(2-pyridylmethyl)aminomethyl] phenol). The characterization of complexes **1** and **2** (mainly by X-ray diffraction and potentiometric titration) led us to study their reactivities toward the hydrolysis of the substrate bis(2,4-dinitrophenyl)phosphate (2,4-BDNPP). These studies revealed that complexes **1** and **2** show the best catalytic activity reported so far, with acceleration rates 8.8×10^4 and 9.95×10^5 times faster, respectively, than the uncatalyzed hydrolysis of 2,4-BDNPP. Catalytic activity of **2** on 2,4-DNPP showed that the monoester is hydrolyzed 27 times slower than the 2,4-BDNPP diester under identical experimental conditions. Therefore, **1** and **2** can undoubtedly be considered highly efficient functional models of the phosphohydrolases.

Introduction

The development of new molecular genetic techniques has stimulated a search for new compounds able to catalytically hydrolyze some of the most important biomolecules, such as proteins, phospholipids, ATP, DNA, and RNA.

The enzymes that naturally hydrolyze phosphodiester bonds in DNA and RNA are called nucleases, and examples are DNA polymerase I, P1 nuclease, and phospholipase C.[1] These enzymes are also called phosphodiesterases and they increase the catalysis rate of the hydrolytic cleavage of the phosphodiester bond by a factor of 10^{12} in relation to the uncatalyzed reaction.[2] The half-life of the phosphodiester bonds in DNA has been estimated as 130,000 years under physiological conditions,[3] and the first-order constants for

* Corresponding author. E-mail: ademir@qmc.ufsc.br. Fax: +55-48-3331-9711.
[†] Laboratório de Bioinorgânica e Cristalografia (LABINC), Departamento de Química, Universidade Federal de Santa Catarina.
[‡] Current address: Departamento de Química Inorgânica, Instituto de Química, Universidade Federal do Rio de Janeiro, 21945-970 Rio de Janeiro, RJ, Brazil.
[§] Laboratório de Equilíbrio Químico, Departamento de Química, Universidade Federal de Santa Catarina.
[||] Technische Universität Darmstadt.
[⊥] Jagiellonian University.

(1) (a) Wilcox, D. E. *Chem. Rev.* **1996**, *96*, 2435−2458. (b) Mitic, N.; Smith, S. J.; Neves, A.; Guddat, L. W.; Gahan, L. R.; Schenk, G. *Chem. Rev.* **2006**, *106*, 3338−3363. (c) Sträter, N.; Lipscomb, W. N.; Klabunde, T.; Krebs, B. *Angew. Chem., Int. Ed. Engl.* **1996**, *35*, 2024−2055.
(2) Sigman, D. S.; Mazumder, A.; Perrin, D. M. *Chem. Rev.* **1993**, *93*, 2295−2316.

10.1021/ic702132t CCC: $40.75
Published on Web 01/09/2008

the single- and double-stranded DNA hydrolysis are estimated as 6×10^{-9} and 6×10^{-10} min^{-1}, respectively.[4]

The search for low molecular weight molecules able to catalytically cleave DNA has attracted much interest among scientists, although a great number of nucleases are well-known. This interest embraces the elucidation of the cleavage mechanism, the role of metals in biological systems, and the design of more effective synthetic hydrolases, as well as the use of these new compounds as catalysts, conformational probes, and synthetic restriction enzymes.[3]

Currently, the strategies for designing new synthetic nucleases are based on natural systems, which usually involve dinuclear active sites, where one of the metal ions is believed to activate the substrate, and the other to act as a Lewis acid, decreasing the pK_a of the coordinated water molecule and stabilizing the accumulated charge over the leaving group. It is also proposed that both metals act together anchoring the substrate and providing the electrostatic stabilization of the five-covalent transition state.[3] On the basis of natural and model systems, Sargenson and co-workers[5] postulated four principles that nowadays represent the bases for developing new complexes as chemical nucleases. The catalytically active site of a synthetic hydrolase should be able to (1) provide two labile sites, *cis*-oriented in order to coordinate the substrate and provide an H_2O/OH^- molecule as the nucleophile; (2) decrease the pK_a of a coordinated water molecule and, as a consequence, provide a hydroxide nucleophile coordinated to the metal at a pH close to neutral; (3) activate the substrate through a nucleophilic attack and/or stabilize the transition state; and (4) release the products at a reasonable rate.

In this regard, our group has been engaged in obtaining mononuclear Cu^{II};[6] binuclear $Cu^{II}Cu^{II}$,[7] $Mn^{III}Mn^{II}$,[8] and $Fe^{III}Fe^{III/II}$;[9] and heterobinuclear $Fe^{III}Ni^{II}$,[10] $Fe^{III}Zn^{II}$,[11] $Fe^{III}Mn^{II}$,[12] and $Fe^{III}Cu^{II}$,[13] complexes which are able to hydrolyze the model substrate 2,4-BDNPP[6,7,9−12] and hydrolytically cleave DNA.[6,7,9,10,13]

Continuing our studies, we describe here the synthesis and characterization of the first $Ni^{II}Ni^{II}$ complex, $[Ni_2(L2)(OAc)_2(CH_3CN)]BPh_4$ (**2**), using the new unsymmetrical dinucleating ligand HL2, (2-(imidazol-4-yl)ethyl)aminomethyl-4-methyl-6-[(2-(pyridyl-2-yl)ethyl)(1-methyl imidazol-2-yl) methyl]aminomethylphenol (Chart 1). We also report the ability of complexes **1**, $[Ni_2(L1)(OAc)_2(H_2O)]ClO_4 \cdot H_2O$,[14] and **2** to catalytically hydrolyze the 2,4-BDNPP model substrate. These studies revealed that **1** and **2** show the best catalytic activity reported so far, with acceleration rates 8.8×10^4 and 9.95×10^5 times faster, respectively, than the uncatalyzed hydrolysis of 2,4-BDNPP.

Experimental Section

Abbreviations are used as follows. HL1, 2-[*N*-bis-(2-pyridylmethyl)aminomethyl]-4-methyl-6-[*N*-(2-pyridylmethyl)amino-methyl]phenol; HL2, 2-[*N*-(2-(pyridyl-2-yl)ethyl)(1-methylimidazol-2-yl)aminomethyl]-4-methyl-6-[*N*-(2-(imidazol-4-yl)ethyl)aminomethyl]phenol; HL3, 2,6-bis[{bis(2-pyridylmethyl)amino}methyl]-4-methyl phenol; HL4, 2,6-bis[{bis(1-methylimidazol-2-y1)amino}methyl]-4-methyl phenol; 2,4-BDNPP, bis(2,4-dinitrophenyl)phosphate; $TBAPF_6$, tetrabutylammonium hexafluorophosphate; 2,4-DNPP, 2,4-dinitrophenyl phosphate; 2,4-DNP, 2,4-dinitrophenolate.

Chart 1. Structures of the Ligands (HL1 and HL2) and Complexes **1** and **2**

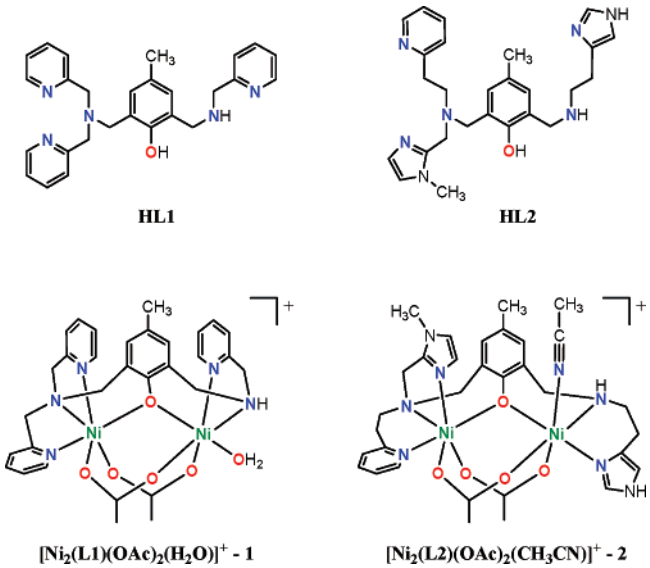

Materials and Measurements. 1-Methyl-2-imidazolecarboxaldehyde,[15] 2-chloromethyl-4-methyl-6-formylphenol,[16] 2,4-BDNPP,[17] 2,4-DNPP,[17,18] and HL1[14] were synthesized by previously described methods. All of the other chemicals and solvents were of analytical or spectroscopic grade purchased from commercial sources, and used without further purification. Infrared spectra were recorded on a Perkin-Elmer model 16PC spectrometer, in KBr pellets in the

(3) Hegg, E. L.; Burstyn, J. N. *Coord. Chem. Rev.* **1998**, *173*, 133−165.
(4) Dong, G.; Zeikus, J. G. *Enzyme Microb. Technol.* **1997**, *21*, 335−340.
(5) (a) Hendry, P.; Sargeson, A. M. *J. Am. Chem. Soc.* **1989**, *111*, 2521−2527. (b) Hendry, P.; Sargeson, A. M. *Prog. Inorg. Chem.* **1990**, *38*, 201−258.
(6) Scarpellini, M.; Neves, A.; Horner, R.; Bortoluzzi, A. J.; Szpoganics, B.; Zucco, C.; Silva, R. A. N.; Drago, V.; Mangrich, A. S.; Ortiz, W. A.; Passos, W. A. C.; Oliveira, M. C. B.; Terenzi, H. *Inorg. Chem.* **2003**, *42*, 8353−8365.
(7) (a) Rossi, L. M.; Neves, A.; Horner, R.; Terenzi, H.; Szpoganics, B.; Sugai, J. *Inorg. Chim. Acta* **2002**, *337*, 366−370. (b) Rossi, L. M.; Neves, A.; Bortoluzzi, A. J.; Hörner, R.; Szpoganicz, B.; Terenzi, H.; Mangrich, A. S.; Pereira-Maia, E.; Castellano, E. E.; Haase, W. *Inorg. Chim. Acta* **2005**, *358*, 1807−1822.
(8) Karsten, P.; Neves, A.; Bortoluzzi, A. J.; Strahle, J.; Maichle-Mossmer, C. *Inorg. Chem. Commun.* **2002**, *5*, 434−438.
(9) Neves, A.; Terenzi, H.; Horner, R.; Horn, A., Jr.; Szpoganicz, B.; Sugai, J. *Inorg. Chem. Commun.* **2001**, *4*, 388−391.
(10) Batista, S. C.; Neves, A.; Bortoluzzi, A. J.; Vencato, I.; Peralta, R. A.; Szpoganicz, B.; Aires, V. V. E.; Terenzi, H.; Severino, P. C. *Inorg. Chem. Commun.* **2003**, *6*, 1161−1165.
(11) Lanznaster, M.; Neves, A.; Bortoluzzi, A. J.; Szpoganicz, B.; Schwingel, E. *Inorg. Chem.* **2002**, *41*, 5641−5643.
(12) Karsten, P.; Neves, A.; Bortoluzzi, A. J.; Lanznaster, M.; Drago, V. *Inorg. Chem.* **2002**, *41*, 4624−4626.
(13) Lanznaster, M.; Neves, A.; Bortoluzzi, A. J.; Aires, V. V. E.; Szpoganicz, B.; Terenzi, H.; Severino, P. C.; Fuller, J. M.; Drew, S. C.; Gahan, L. R.; Hanson, G. R.; Riley, M. J.; Schenk, G. *J. Biol. Inorg. Chem.* **2005**, *10*, 319−332.
(14) Greatti, A.; Brito, M. A.; Bortoluzzi, A. J.; Ceccato, A. S. *J. Mol. Struct.* **2004**, *688*, 185−190.
(15) Oberhausen, K. J.; Richardson, J. F.; Buchanan, R. M.; Pierce, W. *Polyhedron* **1989**, *8*, 659−668.
(16) Uozumi, S.; Furutachi, H.; Ohba, M.; Okawa, H.; Fenton, D. E.; Shindo, K.; Murata, S.; Kitko, D. J. *Inorg. Chem.* **1998**, *37*, 6281−6287.
(17) Bunton, C. A., Farber, S. J. *J. Org. Chem.* **1969**, *34*, 4, 767−772.
(18) Konrad, M.; Meyer, F.; Jacobi, A.; Kircher, P.; Rutsch, P.; Zsolnai, L. *Inorg. Chem.* **1999**, *38*, 4559−4566.

4000−400 cm^{-1} range. Elemental analyses were performed on a Carlo Erba instrument E-1110. Molar conductivities were measured on a Digimed CD-21 conductivimeter at 25 °C. UV−vis spectra were recorded on a Perkin-Elmer Lambda 19 spectrometer.^{1}HNMR spectra were recorded on a Brucker-FT spectrometer (200 MHz) in $CDCl_3$ or CD_3CN and using tetramethylsilane (TMS, $\delta = 0.00$ ppm) as the internal standard. Cyclic voltammograms were recorded with a Princeton Applied Research (PAR) 273 system at room temperature under argon atmosphere. These experiments were carried out employing a standard three-component system consisting of a gold working electrode, a platinum wire auxiliary electrode, and a Ag/AgCl pseudoreference electrode constructed in our laboratory. To monitor the reference electrode, the ferrocenium−ferrocene couple was used.[19] Direct current magnetization data were obtained with a SQUID magnetometer on polycrystalline samples of the complexes **1** and **2**. The samples were pressed into pellets in order to avoid the reorientation of grains in field. The data were corrected for the diamagnetic core contribution as deduced with the use of Pascal's constant tables.[20]

Syntheses. Ligand Syntheses. HL2 was synthesized according the following steps.

(i) [(2-(Pyridyl-2-yl)ethyl)((1-methylimidazol-2-yl)methyl)]-imine (pymimi). This imine was synthesized using a procedure similar to that previously described.[21] 2-(2-Aminoethyl)pyridine (5 mL, 42 mmol) was dissolved in 30 mL of methanol and cooled to 0 °C. A methanolic solution of 1-methyl-2-imidazole carboxaldehyde[15] (3.4 g, 42 mmol, in 10 mL) was added dropwise with stirring. After 3 h, the solvent was removed, and a yellow oil was obtained. IR (film): ν (CH_{Ar} and CH_{Aliph}) 3107−2868; ν ($C{=}N_{imine}$) 1649; ν (C═C and C═N) 1591−1437; ν (C−N) 1103; δ (CH_{Ar}) 761 in cm^{-1}. ^{1}H NMR δ_H (200 MHz; $CDCl_3$): 3.16 [2H, m, CH_2]; 3.87 [3H, s, CH_3]; 3.99 [2H, t, CH_2]; 6.9 [1H, s, CH_{Ar}]; 7.0−7.2 [3H, m, CH_{Ar}]; 7.57 [1H, t, CH_{Ar}]; 8.27 [1H, s, HC═N]; 8.52 [1H, d, CH_{Ar}] in ppm.

(ii) [(2-(Pyridyl-2-yl)ethyl)((1-methylimidazol-2-yl)methyl)]-amine (pymima). A methanolic solution (50 mL) of the Schiff base pymimi was reduced overnight by catalytic hydrogenation using Pd/C (5%). The catalyst was filtered and the solvent removed under reduced pressure giving a slightly yellow oil. A colorless oil was obtained by reduced pressure distillation (55 °C, 0.7 mmHg). Yield: 6.25 g (70%) relative to 2-(2-aminoethyl)pyridine. IR (film): ν (NH_{sec}) 3106; ν (CH_{Ar} and CH_{Aliph}) 3008−2846; ν (C═N and C═C) 1574−1436; ν (C−N) 1110; δ (CH_{Ar}) 756 in cm^{-1}. ^{1}H NMR δ_H (200 MHz; $CDCl_3$): 1.76 [1H, s, NH]; 2.80−2.99 [4H, m, CH_2]; 3.48 [3H, s, CH_3]; 3.74 [2H, s, CH_2]; 6.67 [1H, s, CH_{Ar}]; 6.78 [1H, s, CH_{Ar}]; 6.94−7.04 [2H, m, CH_{Ar}]; 7.44 [1H, t, $J = 7.5$ Hz, CH_{Ar}]; 8.39 [1H, d, $J = 4.6$ Hz, CH_{Ar}] in ppm.

(iii) [(2-(Pyridyl-2-yl)ethyl)((1-methylimidazol-2-yl)methyl)]-aminomethyl]4-methyl -6-formyl-phenol (pymimamfp). To a solution of 2-chloromethyl-4-methyl-6-formylphenol[16] (3.5 g, 19 mmol in 20 mL of CH_2Cl_2), pre-equilibrated at 0 °C was slowly added a solution of triethylamine (2.6 mL, 19 mmol) and pymima (4.2 g, 19 mmol) in 50 mL of CH_2Cl_2 under stirring. After the addition, the ice bath was removed, and the reaction was stirred for 5 h. The desired compound was extracted with 3 × 40 mL of HCl (4 mol L^{-1}). The acid fractions were neutralized with $NaHCO_3$, and extracted with 5 × 30 mL of CH_2Cl_2. The organic layers were dried over anhydrous Na_2SO_4, filtered, and concentrated under reduced pressure to obtain a yellow oil (yield: 85%). IR (film): ν (CH_{Ar} and CH_{Aliph}) 3060−2854; ν (C═O) 1674; ν (C═N and C═C) 1652−1439; δ (OH_{phenol}) 1369; ν (CO_{phenol}) 1278; ν (C−N) 1115; δ (CH_{Ar}) 751 in cm^{-1}. ^{1}H NMR δ_H (200 MHz; $CDCl_3$): 2.26 [2H, s, CH_2]; 2.99 [5H, m, $CH_3 + CH_2$]; 3.41 [2H, s, CH_2]; 3.76 [5H, m, $CH_3 + CH_2$]; 6.76 [1H, s, CH_{Ar}]; 6.94−7.18 [5H, m, CH_{Ar}]; 7.27 [1H, s, CH_{Ar}]; 7.54 [1H, t, $J = 7.54$ Hz, CH_{Ar}]; 8.46 [1H, d, $J = 4.8$ Hz, CH_{Ar}]; 10.15 [1H, s, $CH_{aldehyde}$] in ppm.

(iv) (2-(Imidazol-4-yl)ethyl)aminomethyl-4-methyl-6-[(2-(pyridyl-2-yl)ethyl) (1-methyl-imidazol-2-yl)methyl]aminomethyl-phenol (HL2). A solution of histamine (1.6 g, 14 mmol in 20 mL of CH_2Cl_2) was added dropwise to a solution of the pymimamfp (5.0 g, 14 mmol, in 30 mL of CH_2Cl_2) pre-equilibrated at 0 °C. The reaction was stirred for 3 h in an ice bath, and after that it was reduced overnight by catalytic hydrogenation using Pd/C (5%). The catalyst was filtered and the solvent removed by rotary evaporation to give the crude product, which was dissolved in CH_2Cl_2 and extracted with 3 × 40 mL of HCl (4 mol L^{-1}). The acidic fractions were treated with K_2CO_3 until pH 9 and extracted with 3 × 40 mL of CH_2Cl_2. The organic layers were dried over anhydrous Na_2SO_4 and filtered, and the solvent was removed under reduced pressure without heating to obtain a pale yellow oil (yield: 4.3 g, 67%). IR (film): ν (CH_{Ar} and CH_{Aliph}) 3086−2845; ν (C═N and C═C) 1591−1436; δ (OH_{phenol}) 1366; ν (CO_{phenol}) 1262; ν (C−N) 1108; δ (CH_{Ar}) 750 in cm^{-1}. ^{1}H NMR δ_H (200 MHz; $CDCl_3$): 2.20 [3H, s, CH_3]; 2.82−2.97 [8H, m, CH_2]; 3.41 [3H, s, CH_3]; 3.62−3.92 [6H, m, CH_2]; 4.77 [s, NH]; 6.75−6.84 [4H, m, CH_{Ar}]; 6.92 [1H, s, CH_{Ar}]; 7.01−7.12 [2H, m, CH_{Ar}]; 7.42 [1H, s, CH_{Ar}]; 7.54 [1H, t, $J = 7.65$ Hz, CH_{Ar}]; 8.44 [1H, d, $J = 4.39$ Hz, CH_{Ar}] in ppm.

Safety Note! *Although no problems were encountered during the catalytic hydrogenation reaction, the catalyst (Pd/C) undergoes spontaneous combustion in methanol, and must be handled with care.*

Synthesis of Complexes. $[Ni_2(L1)(OAc)_2(H_2O)]ClO_4 \cdot H_2O$ (1). Complex **1** was synthesized and fully characterized by previously described methods.[14]

$[Ni_2(L2)(OAc)_2(CH_3CN)]BPh_4$ (2). Complex **2** was synthesized in methanolic solution by mixing $Ni(ClO_4)_2 \cdot 6H_2O$ (0.73 g, 2 mmol, in 20 mL) and the HL2 ligand (0.46 g, 1 mmol, in 20 mL) with stirring and mild heating (60 °C). After 15 min, $NaCH_3COO \cdot 3H_2O$ (0.41 g, 3 mmol) was added, and a blue-greenish solution was obtained. $NaBPh_4$ (0.34 g, 1 mmol) was then added, and the reaction was heated (60 °C) under stirring until reduction of the volume to half. The solution was filtered and left to stand for 2 days when a blue-greenish powder was isolated by filtration. Recrystallization in acetonitrile provided single crystals suitable for X-ray crystallographic analysis. Yield: 54% (0.57 g, 0.54 mmol). IR (KBr), in cm^{-1}: ν ($N{-}H_{Ar}$) 3273; ν ($N{-}H_{sec}$) 3160; ν ($C{-}H_{Ar}$ and $C{-}H_{Aliph}$) 3053−2854; ν (C═N and C═C) 1608−1426; ν_{ass} (OAc) 1580; ν_{sym} (OAc) 1442; ν (C−O) 1272; δ ($C{-}H_{Ar}$) 707 and 732. Anal. Calcd for $Ni_2C_{56}H_{61}N_8O_5B$ (Found): C, 63.79 (63.21); H, 5.83 (5.72); N, 10.63 (10.36). $\Lambda_M = 128\ \Omega^{-1} \cdot cm^2 \cdot mol^{-1}$ in CH_3CN.

Caution! *Perchlorate salts with organic ligands are potentially explosive and must be handled in small amounts with care.*

Potentiometric Titrations. The potentiometric studies were carried out with a Corning-350 research pH meter fitted with blue-glass and Ag/AgCl reference electrodes, in ethanol/water (70:30, v/v) solutions, as previously described.[22] All of the experimental solutions were prepared in ethanol/water (70:30, v/v) owing to the

(19) Gagné, R. R.; Koval, C. A.; Lisensky, G. C. *Inorg. Chem.* **1980**, *19*, 2854−2855.
(20) Karlin, R. L. *Magnetochemistry*; Springer-Verlag: Berlin-Heidelberg, 1986; p 3.
(21) Tamboura, F. B.; Gaye, M.; Sall, A. S.; Barry, A. H.; Jouini, T. *Inorg. Chem. Commun.* **2002**, *5*, 235−238.
(22) Schwingel, E. W.; Arend, K.; Zarling, J.; Neves, A.; Szpoganicz, B. *J. Braz. Chem. Soc.* **1996**, *7*, 1, 31−37.

low solubility of the complexes in water. The pK_w of the ethanol/water (70:30% v/v) containing 0.100 mol.L^{-1} of KCl used was 14.72 (2).[22] Computations were carried out with the BEST7[23] program, and species diagrams were obtained with SPE[23] and SPEPLOT[23] programs.

Reactivity. Phosphatase-like activities of complexes **1** and **2** were determined through the hydrolysis reaction of the model substrate bis(2,4-dinitrophenyl)phosphate [2,4-BDNPP] under substrate excess. The experiments were carried out in triplicate and spectrophotometrically monitored at 400 nm (ϵ = 12100 L·mol^{-1}·cm^{-1}) and/or 445 nm (ϵ = 3600 L·mol^{-1}·cm^{-1}) using a Varian Cary 50 BIO UV−vis spectrophotometer coupled to a thermostat bath. The molar extinction coefficients were determined at pH 6.00 and 9.00.[10] Reactions were monitored to less than 5% conversion of 2,4-BDNPP to 2,4-DNP and the data treated using the initial rate method. Initial rates were obtained directly from the plot of the 2,4-dinitrophenolate concentration (2,4-DNP) versus time under the same experimental conditions. In these experiments, all of the solutions were in aqueous/buffer media, except the complex stock solution (3.0×10^{-4} mol·L^{-1} in acetonitrile). Studies regarding the effects of pH on the hydrolysis reaction were performed in the pH range 5.00−12.00 or 5.00−10.00 (MES pH 4.00−6.50; HEPES pH 7.00−8.50; CHES pH 9.00−10.00; KCl/NaOH pH 12.00; I = 0.1 mol.L^{-1} with $LiClO_4$), under a 100-fold excess of substrate, at 25 °C. Experiments to determine the dependence of the reaction rate on the substrate concentration were carried out at 25 °C, pH 9.00 for both substrates (2,4-BDNPP and 2,4-DNPP). In order to establish the number of molecules of substrate which are hydrolyzed per molecule of complex, the reaction was monitored at 445 nm, under a 50-fold substrate excess (5.0×10^{-4} mol·L^{-1}) relative to the complex (1.0×10^{-5} mol·L^{-1}), at pH 9.00 and 25 °C. Also monitored (400 nm) was the stoichiometric reaction (1.0×10^{-5} mol·L^{-1}), at pH 9.00 and 25 °C. The influence of acetate on the reaction rate was evaluated, at pH 9.00, 25 °C, and a 100-fold substrate excess (1.0×10^{-3} mol·L^{-1}) relative to the complex (1.0×10^{-5} mol·L^{-1}). Experiments to determine the dependence of the reaction rate on the complex concentration were carried out at 25 °C, pH 9.00, [2,4-BDNPP] = 3.66×10^{-5} mol·L^{-1}, [complex] = 1.57×10^{-4} to 7.85×10^{-4} mol·L^{-1}, for both complexes. Isotopic effects of deuterium on the hydrolysis of 2,4-BDNPP promoted by complexes **1** and **2** were investigated monitoring parallel reactions, where the buffer solutions CHES pH and pD 9.00 were prepared in H_2O and D_2O, respectively. The reactions were monitored under a 100-fold excess of substrate at 400 and 445 nm, respectively, for complexes **1** and **2**. Also, the effect of temperature on the reaction rate was investigated in the range 20−40 °C at pH 9.00, 25 °C, and a 100-fold substrate excess (1.0×10^{-3} mol·L^{-1}) relative to the complex (1.0×10^{-5} mol·L^{-1}). In all of these experiments, the spontaneous hydrolysis was corrected by direct difference between two identical parallel reactions, unless by the lack of the catalyst in one of them.

Single-Crystal X-ray Structure Determination. The crystallographic analysis was carried out on an Enraf-Nonius CAD4 diffractometer, using graphite monochromated Mo Kα radiation (λ = 0.71069 Å), at room temperature. A blue crystal was selected from a crystalline sample of complex **2** and isolated at the end of a glass fiber for measurement of intensities. Unit-cell parameters were determined from centering of 25 reflections in the θ range 9.82−15.34° and refined by the least-squares method. There were 9738 reflections collected using the $\omega-2\theta$ scan technique. Three standard reflections were monitored every 200 reflections throughout data collection, and no significant intensity decay was observed. All diffracted intensities were corrected for Lorentz and polarization effects. Absorption correction was employed by the ψ-scan method.[24,25] The structure was solved by direct methods and was refined by the full-matrix least-squares method using SHELXS97[26] and SHELXL97[27] computer programs, respectively. All non-hydrogen atoms were refined with anisotropic displacement parameters. The hydrogen atom of the amine group was found from the Fourier map, whereas other H atoms were placed at idealized positions using standard geometric criteria and treated with a riding model. The final refinement of the structure converged to the final indices R = 0.0607 and R_w = 0.1537 for 4908 reflections with [$I > 2\sigma(I)$]. Further relevant crystallographic data are summarized in Table 1.Crystallographic data of complex **2** (atomic coordinates and equivalent isotropic displacement parameters, calculated hydrogen atom parameters, anisotropic thermal parameters and bond lengths and angles) have been deposited at the Cambridge Crystallographic Data Center (deposition number CCDC 628592). Copies of this information may be obtained free of charge from: CCDC, 12 Union Road, Cambridge, CB2 1EZ, U.K. (Fax: +44-1223-336-033. E-mail: deposit@ccdc.cam.ac.uk or http://www.ccdc.cam.ac.uk).

Table 1. Crystallographic Data for Complex **2**

empirical formula	$C_{56}H_{61}BN_8Ni_2O_5$
fw (g·mol^{-1})	1054.36
T (K)	293(2)
wavelength (Å)	0.71073
crystal system	monoclinic
space group	$P2_1/c$
unit cell dimensions	
a (Å)	15.059(1)
b (Å)	16.797(2)
c (Å)	22.259(3)
β (deg)	108.34(1)
V (Å^3)	5344.3(10)
Z/calcd density (g·cm^3)	4/1.310
abs coeff (mm^{-1})	0.760
F(000)	2216
cryst size (mm^3)	0.43 × 0.30 × 0.26
θ range for data collection (deg)	2.28−25.07
limiting indices	$-17 \le h \le 17$
	$0 \le k \le 20$
	$0 \le l \le 26$
reflns collected/unique	9738/9471 (R_{int} = 0.0429)
abs correction	ψ-scan
max and min transm	0.823 and 0.772
refinement method	full-matrix least-squares on F^2
data/restraints/params	9471/0/652
extinction coeff	0.0011(3)
GOF on F^2	1.009
final R indices [$I > 2\sigma(I)$]	R = 0.0607, R_w = 0.1537
R indices (all data)	R = 0.1700, R_w = 0.1961
residual electronic density (e Å^3)	0.433 and −0.723

Results and Discussion

Syntheses. HL2 is a completely unsymmetrical dinucleating ligand containing two types of imidazole and pyridine residues while ligand HL1 contains only pyridine residues.[14] HL2 was synthesized by typical procedures starting from

(23) Martell, A. E.; Motekaitis, R. J. *Determination and Use of Stability Constants*, 2nd ed.; VHC Publishers, Inc.: Weinheim, 1992.

(24) Spek, A., L. *PLATON: Molecular Geometry and Plotting Program*; University of Utrecht: The Netherlands, 1997.

(25) North, A. C. T.; Phillips, D. C.; Mathews, F. S. *Acta. Crystallogr.* **1968**, *A24*, 351−359.

(26) Sheldrick, G. M. *SHELXS-97: Program for the Solution of Crystal Structures*; University of Göttingen: Göttingen, Germany, 1990.

(27) Sheldrick, G. M. *SHELXL-97: Program for the Refinement of Crystal Structures*; University of Göttingen: Göttingen, Germany, 1997.

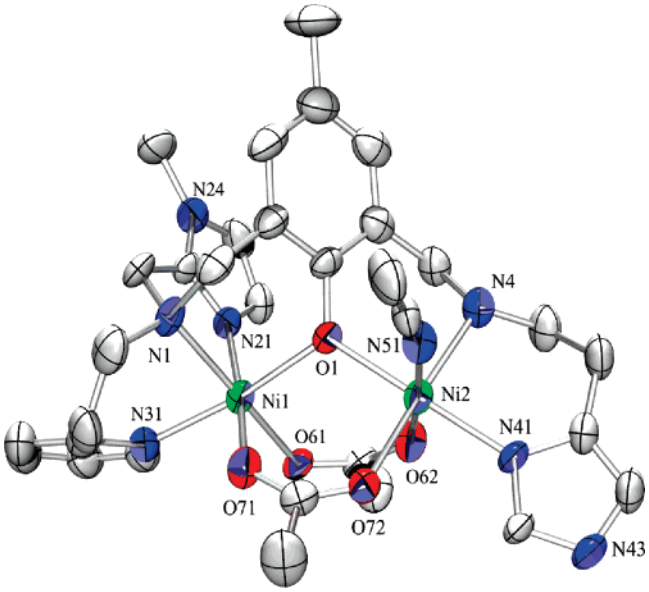

Figure 1. *ORTEP*[29] view of complex **2**, showing the atom labeling and 40% probability ellipsoids.

Table 2. Main Bond Distances (Å) and Angles (deg) for Complex **2**

Ni1−O71	2.023(4)	Ni2−O1	2.034(4)
Ni1−O1	2.037(4)	Ni2−O62	2.038(4)
Ni1−O61	2.068(4)	Ni2−O72	2.052(4)
Ni1−N21	2.069(5)	Ni2−N41	2.078(4)
Ni1−N31	2.175(5)	Ni2−N51	2.080(5)
Ni1−N1	2.188(5)	Ni2−N4	2.127(5)
O71−Ni1−O1	92.70(17)	O62−Ni2−N41	91.49(18)
O71−Ni1−O61	94.73(17)	O72−Ni2−N41	86.99(18)
O1−Ni1−O61	92.52(15)	O1−Ni2−N51	85.56(18)
O71−Ni1−N21	173.24(19)	O62−Ni2−N51	175.56(19)
O1−Ni1−N21	88.66(17)	O72−Ni2−N51	86.13(19)
O61−Ni1−N21	91.83(18)	N41−Ni2−N51	92.94(19)
O71−Ni1−N31	93.44(19)	O1−Ni2−N4	90.25(17)
O1−Ni1−N31	172.37(18)	O62−Ni2−N4	89.3(2)
O61−Ni1−N31	91.50(18)	O72−Ni2−N4	175.21(19)
N21−Ni1−N31	84.73(19)	N41−Ni2−N4	89.80(19)
O71−Ni1−N1	92.02(19)	N51−Ni2−N4	90.5(2)
O1−Ni1−N1	90.62(18)	C12−O1−Ni2	121.9(3)
O61−Ni1−N1	172.41(18)	C12−O1−Ni1	120.1(3)
N21−Ni1−N1	81.3(2)	Ni2−O1−Ni1	117.78(19)
N31−Ni1−N1	84.6(2)	C63−O61−Ni1	132.2(4)
O1−Ni2−O62	90.01(16)	C63−O62−Ni2	131.5(4)
O1−Ni2−O72	92.87(16)	C73−O71−Ni1	129.9(4)
O62−Ni2−O72	94.29(18)	C73−O72−Ni2	135.1(4)
O1−Ni2−N41	178.50(18)		

the phenol nucleous 2-chloromethyl-4-methyl-6-formylphenol,[16] in good yield, and in a purity sufficient for use without further purification. HL2 is able to coordinate two Ni^{II} ions held together by one endogenous phenoxo bridge and two exogenous acetate groups. Infrared spectroscopy was essential for the preliminary characterization of the ligands and complexes. The exogenous acetate coordination mode being bidentate[28] in complex **2** was inferred by the difference between the asymmetric and symmetric stretching ($\Delta = \nu_{asym} - \nu_{sym} \sim 138$ cm^{-1}) bands, which were assigned by the difference between the spectra of complex **2** and HL2. It was also useful to identify the presence of the acetonitrile molecule through the CN stretching at ~ 2300 cm^{-1}.[28]

X-ray Structural Characterization. Complex **2** crystallizes as blue single crystals that belong to the monoclinic crystal system and space group $P2_1/c$. An ORTEP[29] view of the cation complex is presented in Figure 1. The crystallographic data and the main bond distances/angles are given in Tables 1 and 2, respectively. The resolution of the crystal structure of **2** shows an asymmetric unit composed of a cation complex $[Ni_2(L2)(OAc)_2(CH_3CN)]^+$ and a tetraphenylborate anion as the counterion.

Figure 1 shows the structure of the cation complex which is composed of one unsymmetrical ligand L2 coordinated to two Ni^{II} atoms (Ni1 and Ni2). Each Ni^{II} center is six-coordinated and bridged by two exogenous acetate groups coordinated in the bidentate mode, and by the phenoxo endogenous bridge. Both Ni^{II} centers are in an N_3O_3 coordination environment arranged in distorted octahedral geometries, as evidenced by all of the angles around them that deviate from 180° and 90° (Table 2). The Ni1 center is bound to three nitrogen atoms [N1 (tertiary amine), N21 (imidazole), and N31 (pyridine)], which are arranged in a facial mode and belong to the pendant arm of the binucleating ligand L2. Besides the nitrogen atoms, the coordination sphere of the Ni1 center is completed by three oxygen atoms, O61 and O71, provided by the exogenous acetate bridges, and O1 from the endogenous phenoxo. The coordination sphere of the Ni2 center is composed of the amine nitrogen N4, *trans* positioned to the oxygen atom O72, the nitrogen imidazole N41 *trans* to the oxygen O1, and the nitrogen N51 (from an acetonitrile molecule) *trans* to the oxygen O62 (from an acetate bridge).

As shown in Chart 1, complexes **1** and **2** are similar in the sense that both are derived from unsymmetrical binucleating N_5O ligands (HL1 and HL2). However, the crystal structures of complexes **1**[14] and **2** (Figure 1) show a difference in the coordination sphere of the Ni2 center. In complex **2**, the nitrogen atom N41 from the pendant arm is *trans* positioned to the oxygen O1 from the phenoxo bridge, whereas in complex **1** this position is occupied by a terminal water molecule. This inversion in the coordination of the pendant arms of ligands L1 and L2 with terminal solvent molecules is related to the presence of two methylenic groups as spacers of the two nitrogen donors (amine and imidazole) in the pendant arm of the L2 ligand. Ligands such as L1 containing just one methylenic group as the spacer form five-membered rings when coordinated to a metal center, which are known to be more constrained than six-membered rings. Confirming the fact that the tension of the six-membered chelate rings is less than that of the five-membered ones, the angle N4−Ni2−N41 (89.80(19)°) in complex **2** is 8.76° greater than the corresponding angle in complex **1** N4−Ni2−N42 (81.05(16)°).[14] As observed in complex **1**,[14] the average bond distances Ni−N (2.120 Å) and Ni−O (2.042 Å) in **2** are in the range of values reported for this kind of bond in dinuclear Ni^{II} complexes.[30−32] The bond distances Ni1−O1

(28) Nakamoto, K. *Infrared and Raman Spectra of Inorganic and Coordination Compounds*, 3rd ed.; John Wiley & Sons, Inc.: New York, 1977; Part III, pp 231−232, 242.
(29) Farrugia, L. J. *J. Appl. Crystallogr.* **1997**, *30*, 565.
(30) Buchanan, R. M.; Mashuta, M. S.; Oberhausen, K. J.; Richardson, J. F.; Li, Q.; Hendrickson, D. N. *J. Am. Chem. Soc.* **1989**, *111*, 4497−4498.

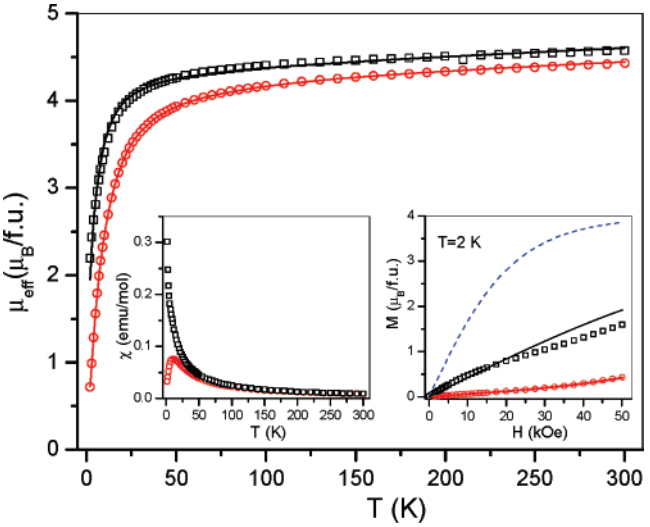

Figure 2. Main panel: temperature dependence of the effective magnetic moment for complexes **1** (○) and **2** (□). Left inset: temperature dependence of the molar susceptibility for the two complexes. Right inset: magnetic moment per formula unit vs magnetic field. The dashed line is the Brillouin curve for two free spins $S = 1$, which is shown for comparison. Solid lines are fits.

(2.037(4) Å) and Ni2−O1 (2.034(4) Å) are slightly longer than those observed in complex **1** (2.001(3) Å), although those of Ni−O−Ni are similar. The distance Ni1···Ni2 (3.486(1) Å) in complex **2** is also slightly longer than in complex **1** (3.431(1) Å), but even closer to those observed in the metalloenzyme urease from *Klebisiella aerogenes* (3.5 Å)[33] and *Bacillus pasteuri* (3.7 Å).[34] All of these structural features lead us to consider complexes **1** and **2** as structural models of the hydrolase enzyme class called ureases.

Magnetic Properties of 1 and 2. The magnetic data for complexes **1** and **2** were obtained both as a function of temperature as well as a function of the magnetic field.

The variable temperature data were collected in the temperature range 2.0−300 K at a constant magnetic field (10000 Oe for **1** and 1000 Oe for **2**). The variable field data were collected in the field range 0−50 kOe at a temperature of 2 K. The experimental temperature dependence of the effective magnetic moment $\mu_{eff} = 2.828\ (\chi_{mol}T)^{1/2}$ is shown in Figure 2 in the main panel. Temperature dependence of the molar susceptibility χ_{mol} is shown in the left inset. The magnetization versus field dependence $M(H)$ (in μ_B per formula unit) is shown in the right inset. These results indicate the presence of antiferromagnetic exchange interaction between the Ni(II) centers for both complexes and show that the exchange coupling for **1** is stronger than for **2**. The latter is clearly seen from the right inset, where $M(H)$ curves for both substances are compared with the $M(H)$ curve for uncoupled spins.

A detailed analysis was carried out using the following Hamiltonian

$$\mathbf{H} = -J\,\hat{\mathbf{S}}_1\cdot\hat{\mathbf{S}}_2 - \hat{\mathbf{S}}_1\cdot\hat{\mathbf{D}}_1\cdot\hat{\mathbf{S}}_1 - \hat{\mathbf{S}}_2\cdot\hat{\mathbf{D}}_2\cdot\hat{\mathbf{S}}_2 - \mu_B\mathbf{H}(\hat{\mathbf{g}}_1\hat{\mathbf{S}}_2 + \hat{\mathbf{g}}_2\hat{\mathbf{S}}_2) \quad (1)$$

where $\hat{\mathbf{S}}_i$ ($S_i = 1$; $i = 1, 2$) are spin operators, $\hat{\mathbf{D}}_i$ are tensor operators of the zero field splitting, and $\hat{\mathbf{g}}_i$ are tensors of the spectroscopic factors. The local coordinate systems were chosen so that their axes are principal axes of the $\hat{\mathbf{D}}_i$ tensors. It was assumed that the principal axes of the $\hat{\mathbf{g}}_i$ tensors are the same as of the $\hat{\mathbf{D}}_i$ tensors and that the principal z-axes form the angle, it being close to the angle Ni1−O1−Ni2 or to its completion to 180°. The local symmetry was approximated as axial in order to limit the number of parameters. The parameters were found using our general program for fitting magnetic susceptibility and/or magnetization of small spin clusters. Standard quantum statistical mechanics was used, in which spins in the Hamiltonian were represented by Pauli matrices, from which by direct products the matrices were constructed corresponding to the proper dimension of the Hilbert space. The Hamiltonian matrix was numerically diagonalized after transformation to the common molecular system using routines from the IMSL mathematical library. Temperature and field dependencies were fitted simultaneously. With this procedure there is a chance that the unambiguous solution can be obtained with the proper sign of **D** parameters because the magnetization data are more sensitive to this sign.[35]

According to the Hamiltonian, the magnetic properties of **1** can be simulated as indicated by the solid curves in Figure 2, using the following magnetic parameters: $J = -8.5 \pm 1.4\ cm^{-1}$, $D_1 = D_2 = -2.3 \pm 1.4\ cm^{-1}$, $g_1 = g_2 = 2.10 \pm 0.02$, TIP (temperature-independent paramagnetism) $= 9 \times 10^{-4}\ cm^3\ mol^{-1}$. Correspondingly, the parameters for **2** follow: $J = -3.4 \pm 0.02\ cm^{-1}$, $D_1 = D_2 = -8.4 \pm 2.8\ cm^{-1}$, $g_1 = g_2 = 2.18 \pm 0.02$, TIP $= 1 \times 10^{-3}\ cm^3\ mol^{-1}$. The parameters D_1, D_2 and g_1, g_2 were inserted in the last fit as equal, because they differed only in the limits of statistical uncertainties. The obtained solutions were weakly dependent on the angle between principal axes in the broad limits of this angle. The fit of $M(H)$ dependence for **2** is not perfect and could not be improved by introducing more parameters, as orthorhombicity parameter E, intermolecular interaction or anisotropic orientation of grains. The reason for this is unknown. The fits with the negative values of D parameters were of remarkably better quality.

In fact, it has been observed that, for related complexes containing the {Ni^{II}(μ-phenoxo)(OAc)$_2$Ni^{II}}, {Ni^{II}(μ-phenoxo)(OAc)Ni^{II}}, or {Ni^{II}(μ-phenoxo)(NCS)Ni^{II}} moieties, the magnetic interaction is generally weak and varies from antiferromagnetism to ferromagnetism on introducing slight changes in the nature of the dinuclear core.[36] However, the authors were unable to identify any dominant factor con-

(31) Brito, M. A.; Bortoluzzi, A. J.; Greatti, A.; Ceccato, A. S.; Joussef, A. C.; Drechsel, S. M. *Acta Crystallog.* **2000**, *C56*, 1188−1190.
(32) Adams, H.; Bradshaw, D.; Fenton, D. E. *Inorg. Chim. Acta* **2002**, *332*, 195−200.
(33) Jabri, E.; Carr, M. B.; Hausinger, R. P.; Karplus, P. A. *Science* **1995**, *268*, 998−1004.
(34) Benini, S.; Rypniewski, W. R.; Wilson, K. S. Miletti, S.; Ciurli, S.; Magani, S. *Structure* **1999**, *7*, 205−216.
(35) (a) Ginsberg, A. P.; Martin, R. L.; Brookes, R. W.; Sherwood, R. C. *Inorg. Chem.* **1972**, *11*, 2884−2889. (b) Bŏca, R.; Dlhá, L.; Haase, W.; Herchel, R.; Mašlejová, A.; Papánková, B. *Chem. Phys. Lett.* **2003**, *373*, 402−410.

tributing to the positive or negative exchange constant from inspection of the crystal structures of a series of four dinuclear Ni(II) complexes. For the complexes presented here, which have a common $\{Ni^{II}(\mu\text{-phenoxo})(OAc)_2Ni^{II}\}$ structural unit, one can observe that despite the small differences in the Ni1−O1−Ni2 bond angles (118.01° for **1** and 117.8° for **2**) and the average Ni−O1 bridging bond lengths (2.001 Å for **1** and 2.036 Å for **2**), these most probably account for the stronger antiferromagnetic coupling observed for complex **1**. Furthermore, the data are in agreement with the antiferromagnetic magnetic interactions found in the related complexes $[Ni_2(L3)(OAc)_2]ClO_4$[32] and $[Ni_2(L4)(OAc)_2)]ClO_4$,[30] for which $J = -4.6$ cm^{-1} (Ni1−O1−Ni2 = 114.5°, Ni−O = 2.022 Å) and $J = -3.8$ cm^{-1} (Ni1−O1−Ni2 = 116.7°, Ni−O = 2.010 Å), have been reported, respectively. Nevertheless, all attempts to find a linear magneto-structural (J vs Ni−O−Ni angle) correlation for complexes **1** and **2**, and for $\{Ni^{II}(\mu\text{-phenoxo})(OAc)_2Ni^{II}\}$, $\{Ni^{II}(\mu\text{-phenoxo})(OAc)Ni^{II}\}$ previously described in the literature, were unsuccessful. Therefore, it is concluded that further fully characterized dinuclear Ni(II) complexes containing the common $\{Ni^{II}(\mu\text{-phenoxo})(OAc)_2Ni^{II}\}$ structural unit are necessary to identify and evaluate the electronic and structural factors influencing the exchange constant.

Electronic Spectroscopy and Electrochemical Properties. UV−vis spectra of complex **2** were recorded in the solid state (diffuse reflectance in MgO pellet) and in solution (CH_3CN) in order to investigate the occurrence of any change in the coordination sphere of the complex when it is dissolved (Figure S1). For the MgO pellet, the spectrum is composed of bands at 624, 771, and 1010 nm, which are very similar to those observed in solution (CH_3CN, 5.0×10^{-5} mol·L^{-1}) and are at 303 ($\epsilon = 3852$ mol·L^{-1}·cm^{-1}), 624 ($\epsilon = 19$ mol·L^{-1}·cm^{-1}), 769 ($\epsilon = 5$ mol·L^{-1}·cm^{-1}), and 1015 ($\epsilon = 19$ mol·L^{-1}·cm^{-1}) nm. As observed, all of the bands have low molar absorptivity coefficients indicating ligand field (d−d) transitions, except that at 303 nm. Usually, Ni^{II} complexes in octahedral environments show three spin-allowed d−d transitions in the ranges 1250−900, 670−520, and 500−370 nm with low molar absorptivity coefficients (<30 mol·L^{-1}·cm^{-1}).[37] On the basis of this information, the spectra of complex **2** (Figure S1) are consistent with octahedral environments for both Ni^{II} centers either in the solid state or in solution, and are in agreement with the X-ray analysis. The spectra have two broad bands in the ranges 670−520 and 1250−900 nm, which can be attributed to the $^3A_{2g} \rightarrow {}^3T_{2g}$ (F) and $^3A_{2g} \rightarrow {}^3T_{1g}$ (F) transitions, respectively.[37] On the other hand, the weak absorption observed around 700 nm is attributed to a spin-forbidden transition: $^3A_{2g}$ (F) $\rightarrow {}^1E_g$ (D). In addition to these transitions, another band is observed at 303 nm, which can be attributed to a charge-transfer transition involving orbitals from Ni^{II} and the pyridine ligand, as previously observed for complex **1**[14] and other Ni^{II} complexes.[38−40]

The redox properties of complexes **1** and **2** were investigated by cyclic voltammetry which revealed the presence of two irreversible anodic waves (Figure S2) in CH_2Cl_2 at 100 mV/s, with Fc^+/Fc as the internal standard. The peaks at $E_{ox1} = 1.04$, $E_{ox2} = 1.20$ for complex **1** and $E_{ox1} = 0.73$, $E_{ox2} = 0.94$ V for complex **2** (vs NHE) are assigned to the irreversible stepwise one-electron oxidation couples $Ni^{II}Ni^{II}/Ni^{II}Ni^{III}$ and $Ni^{II}Ni^{III}/Ni^{III}Ni^{III}$, respectively. This redox behavior is also displayed by other dinuclear Ni^{II} complexes,[40] and the cathodic shift observed for complex **2** when compared to complex **1** reflects the greater donating ability of HL2 in relation to HL1, which decreases the redox potential as the electronic density over the metal center in **2** increases. Interestingly, the difference between E_{ox1} for **1** and **2** is 0.3 V while that for the second oxidation process, E_{ox2}, is only slightly decreased to 0.25 V. Such an observation is in full agreement with the distinct coordination environments around the Ni(II) centers in **1** and **2**. In fact, the greater difference observed for E_{ox1} most probably is a reflection of the distinct basic character of the 2-methylpyridyl and 1-methylimidazole pendant arms in **1** and **2**, respectively (five-membered rings), while the smaller difference detected for E_{ox2} is primary associated with the same influence but is partially compensated due to the six-membered ring formed with the 2-ethylpyridyl and histamine pendant arms in **2**.[41]

Potentiometric Equilibrium Studies. Potentiometric titrations of complexes **1** and **2** were carried out in ethanol/water (70:30% v/v) solutions because of the low solubility of these compounds in pure water. These experiments were carried out to assess the presence of water molecules coordinated to the Ni^{II} metal centers when in solution, as the lability of the acetate bridges has been reported.[10,11,13] This labilization is favored when the pH of the solution is increased, and consequently, aquo-complexes are generated.[10,11,13] The results obtained for the two complexes show the neutralization of 2 mol KOH per mol of complex in the pH range 5.00−11.00. Treating the data, two deprotonation constants were obtained for each complex which were defined from eqs 2 and 3, and are reported in Table 3. Figure

Table 3. pK_a Values for Complexes **1** and **2**

complex	pK_{a1}	pK_{a2}
1	5.98 ± 0.06	9.7 ± 0.3
2	6.65 ± 0.04	8.2 ± 0.2

(36) (a) Koga, T.; Furutachi, H.; Nakamura, T.; Fukita, N.; Ohba, M.; Takahashi, K.; Ökawa, H. *Inorg. Chem.* **1998**, *37*, 989−996. (b) Carlsson, H.; Haukka, M.; Bousseksou, A.; Latour, J.-M.; Nordlander, E. *Inorg. Chem.* **2004**, *43*, 8252−8262.

(37) Lever, A. B. P. *Inorganic Electronic Spectroscopy*, 2nd ed.; Elsevier Science Publishers B.V.: Amsterdam, 1984; pp 553−572.

(38) Uozumi, S.; Furutachi, H.; Ohba, M.; Okawa, H.; Fenton, D. E.; Shindo, K.; Murata, S.; Kitko, D. J. *Inorg. Chem.* **1998**, *37*, 6281−6287.

(39) Barefield, K. E.; Lovecchio, F. V.; Nurhan, E. T.; Ochiai, E.; Busch, D. H. *Inorg. Chem.* **1972**, *11*, 283−288.

(40) (a) Holman, T. R.; Hendrich, M. P.; Que, L., Jr. *Inorg. Chem.* **1992**, *31*, 937−939. (b) Gultneh, Y.; Khan, A. R.; Ahvazi, B.; Butcher, R. J. *Polyhedron* **1998**, *17*, 3351−3360.

(41) (a) Neves, A.; Brito, M. A.; Vencato, I.; Drago, V.; Griesar, K.; Haase, W. *Inorg. Chem.* **1996**, *35*, 2360−2368. (b) Kessissoglou, D. P.; Li, X.; Butler, W. M.; Pecoraro, V. L. *Inorg. Chem.* **1987**, *26*, 2487−2492.

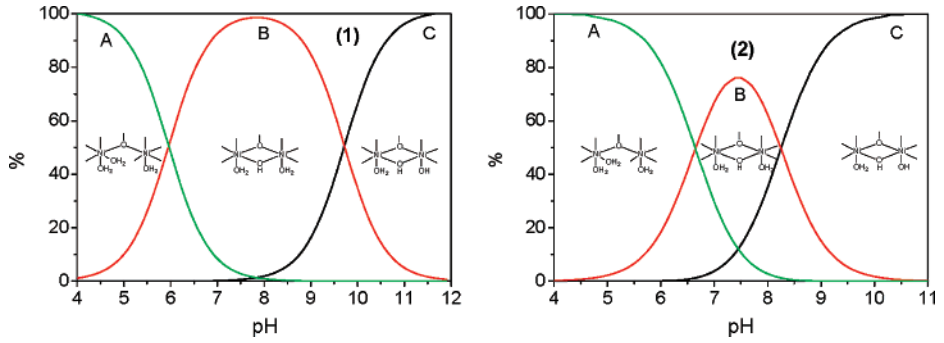

Figure 3. Species distribution curves of complexes **1** and **2** as a function of pH.

Chart 2. Proposed Equilibria Observed for Complexes **1** and **2** in Solution

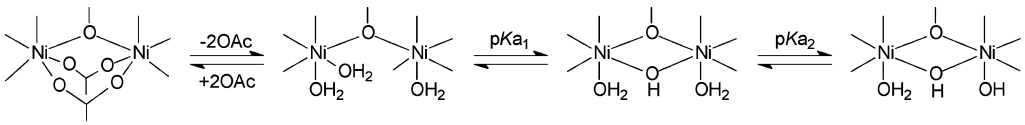

3 shows the species distribution curves as a function of pH for complexes **1** and **2**.

$$[(OH_2)Ni^{II}(OH_2)Ni^{II}(OH_2)] \overset{pK_{a1}}{\rightleftharpoons} [(OH_2)Ni^{II}(OH)Ni^{II}(OH_2)] + H^+ \quad (2)$$

$$[(OH_2)Ni^{II}(OH)Ni^{II}(OH_2)] \overset{pK_{a2}}{\rightleftharpoons} [(OH_2)Ni^{II}(OH)Ni^{II}(OH)] + H^+ \quad (3)$$

The first deprotonation constant can be tentatively attributed to the formation of a species containing a hydroxo bridge, immediately after the hydrolysis of the acetate groups (Chart 2).

This attribution is based on the fact that the pK_a value observed here is significantly lower than the value reported[42] for the first water deprotonation constant (pK_a = 10.2) for the complex $[Ni(H_2O)_6]^{2+}$, this being a reflection of the cooperative effect of both Ni^{II} centers on the same water molecule. In addition, μ-hydroxo species have been observed at pH ~ 6 for $Fe^{III}Ni^{II}$,[10] $Fe^{III}Zn^{II}$,[11] $Fe^{III}Cu^{II}$,[13] $Ga^{III}Ni^{II}$,[43] and $Ga^{III}Zn^{II}$ [44] systems. As can be observed in Table 3, the second titratable proton in complex **1** has a pK_a value approximately one and a half units higher than the corresponding value for complex **2**. This suggests that these values are related to the deprotonation of different water molecules coordinated to the Ni^{II} centers. It is well-known that the relative acidity of coordinated water molecules is usually associated with the influence of the donor atom *trans* positioned to them in the coordination sphere of the metal center. The longer the metal−donor atom bond distance, the higher the metal−water interaction, and the lower the observed pK_a value. In view of this, on looking for a correlation between the pK_{a2} values and structural data for complexes **1** and **2**, it was observed that the Ni1 centers are very similar considering both the coordination of N-donor groups and the bond distance averages. In the Ni2 center, bond distance averages are also analogous. However, the N-donor groups differ in the coordination mode, probably because of the increase in the linker group between the amine nitrogen (N4) and the aromatic nitrogen atoms (5-membered and 6-membered rings for **1** and **2**, respectively). On the basis of these structural differences, it is suggested that the second pK_a for both complexes **1** and **2** is related to the deprotonation of the water molecule coordinated to the Ni2 center. Considering that the hexadentate ligands HL1 and HL2 maintain their coordination mode in complexes **1** and **2** in solution, it is suggested that the second titratable proton originates from the water molecule *trans* positioned to the pyridine (N42) nitrogen atom in complex **1**. This group presents higher donation ability when compared to the water ligand in complex **2** (vide infra). Thus, the metal acquires a lower Lewis acid character, and consequently, a higher pK_a is observed. In turn, the second pK_a in complex **2** is attributed to the deprotonation of a water molecule *trans* positioned to another water molecule, as a consequence of the lability of the acetonitrile ligand in solution. In Figure 3, it is observed that species B, $[(OH_2)Ni(OH)Ni(OH_2)]$, achieves maximum values of 97.4% at pH 7.81, and 76.6% at pH 7.41, for complexes **1** and **2**. As the pH increases, another deprotonation is observed giving rise to species C, $[(OH_2)Ni(OH)$-$Ni(OH)]$, which is predominant at pH values higher than 9.7 and 8.2 for complexes **1** and **2**, respectively.

Reactivity Studies. Although complexes **1** and **2** are structural models for ureases, difficulties associated with the monitoring of urea hydrolysis have led scientists to test dinickel(II) model complexes in the hydrolysis of phosphate esters.[45−48] Thus, kinetics experiments were carried out to

(42) Smith, R. M.; Martell, A. E.; Motekaitis, N. *Critical stability constants of metal*, database version 5.0; NIST Standard Reference Database 46, U.S. Department of Commerce: Gaithersburg, MD, 1995.
(43) Batista, S. C. Ph.D. Thesis, Federal University of Santa Catarina, Florianópolis, Brazil, 2003, p 161.
(44) Casellato, A. Master Thesis, Federal University of Santa Catarina, Florianópolis, Brazil, 2003, p 63.
(45) Volkmer, D.; Hommerich, B.; Griesar, K.; Haase, W.; Krebs, B. *Inorg. Chem.* **1996**, *35*, 3792−3803.
(46) Hosokawa, Y.; Yamane, H.; Nakao, Y.; Matsumoto, K.; Takamizawa, S.; Mori, W.; Suzuki, S.; Kimoto, H. *Inorg. Chim. Acta* **1998**, *283*, 118−123.
(47) Hommerich, B.; Schoepp, H.; Volkmer, D.; Krebs, B. *Z. Anorg. Allg. Chem.* **1999**, *625*, 75−82.

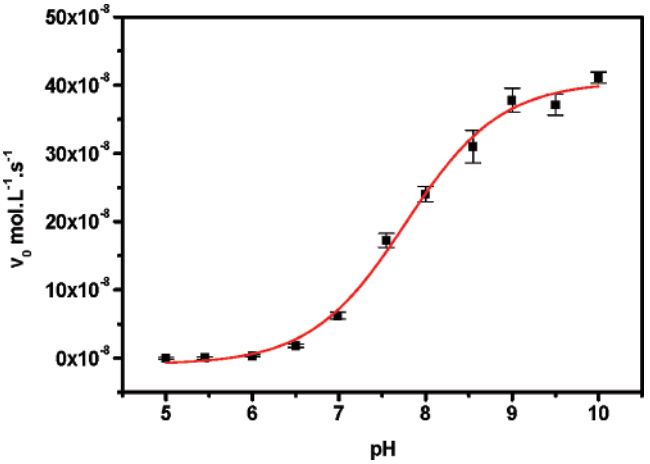

Figure 4. Dependence of the initial reaction rate (υ_0) on pH for the hydrolysis of 2,4-BDNPP promoted by complex **2**. [Complex] = 1.0 × 10^{-5} mol·L^{-1}; [2,4-BDNPP] = 1.0 × 10^{-3} mol·L^{-1}; [buffers] = 50.0 × 10^{-3} mol·L^{-1}; I = 50.0 × 10^{-3} mol·L^{-1} ($LiClO_4$) in H_2O/CH_3CN (50% v/v) at 25 °C.

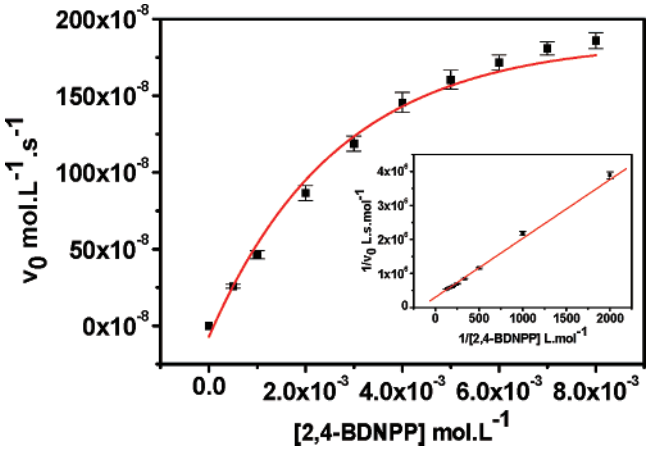

Figure 5. Dependence of the initial reaction rate (υ_0) on the 2,4-BDNPP concentration for the hydrolysis reaction promoted by complex **2**. Conditions: [complex] = 1.0 × 10^{-5} mol·L^{-1}; [buffer] = 50.0 × 10^{-3} mol·L^{-1} (CHES, pH = 9.00); I = 50.0 × 10^{-3} mol·L^{-1} ($LiClO_4$) in H_2O/CH_3CN (50% v/v) at 25 °C.

assess the ability of complexes **1** and **2** to hydrolyze the substrate 2,4-BDNPP.[17] The hydrolysis activities were investigated in the pH range 5.00−12.00 and 5.00−10.00, respectively, for complexes **1** and **2**. As shown in Figures 4 and S3 (Supporting Information), the initial rate (υ_0) versus pH plots for the two complexes have sigmoidal shapes. These curves were fitted by the Boltzman model and the kinetic pK_a values determined: complex **1**, pK_a 9.2 ± 0.1, and complex **2**, pK_a 7.8 ± 0.1. These values, obtained in H_2O/CH_3CN (50% v/v), are in reasonable agreement with those determined by potentiometric titration in EtOH/H_2O (70:30% v/v): complex **1**, pK_a 9.7 ± 0.3, and complex **2**, pK_a 8.2 ± 0.2. This agreement between the kinetic and the potentiometric pK_a values reinforces the proposal that deprotonation of a coordinated water molecule is necessary to generate the catalytically active aqua-hydroxo [$(OH_2)Ni^{II}(\mu$-$OH)Ni^{II}(OH)$] species (eq 2) (see also Figure S4). Data obtained from these experiments also revealed that υ_0 is highly influenced by alkaline pH, since for a difference of only two pH units (6.00−8.00, for example) the reaction rate increases by a factor of 17 and 69, respectively, for complexes **1** and **2**.

The effect of the substrate 2,4-BDNPP concentration on the hydrolysis rate promoted by complexes **1** and **2** was also investigated, and the experiments were carried out at pH 9.00 and 25 °C (Figures 5 and S5).

As can be observed in Figure 5 for complex **2** (and Figure S5 for complex **1**), the dependence of the initial reaction rate (υ_0) on the 2,4-BDNPP concentration plots shows a linearity at low substrate concentrations, and attains a saturation curve as the concentration increases, which suggest the formation of an intermediate complex−substrate. In view of this behavior, the Michaelis−Menten[49] model was employed, and the data were fit by the Lineweaver−Burk linearization method. The double-reciprocal plots (1/[2,4-BDNPP] vs 1/υ_0) are presented in the inset of Figure 5 for complex **2** (and Figure S5 for complex **1**). The kinetics parameters for the 2,4-BDNPP hydrolysis promoted by complexes **1** and **2** are given in Table 4, where it can be observed that complex **2** is most effective in the conversion of substrate to products, with a catalytic activity in the hydrolysis 9.95 × 10^5 times faster than the uncatalyzed reaction (k_{nc} = 3.88 × 10^{-7} s^{-1} at 25 °C).[17] This data can be addressed considering two factors: (i) At pH 9.00, complex **1** has approximately 17% of the active species, whereas complex **2** has ca. 85% (Figure 2), which means a higher effective concentration of the active species for complex **2,** which is probably related to the faster hydrolysis rate observed. (ii) By way of structural remarks, complex **2** possesses two six-membered rings, which in the complex−substrate intermediate are probably *cis* positioned to the terminal hydroxide ion and to the substrate. This proximity between the nucleophile and the substrate should facilitate the nucleophilic attack on the phosphorus atom resulting in a more efficient catalytic process.

In order to assess the possible hydrolysis of the monoester 2,4-DNPP, one of the products formed from the hydrolysis reaction of the diester 2,4-BDNPP, a stoichiometric reaction between complex **1** (and **2**) and the 2,4-BDNPP substrate (Figure S6), was monitored. It was observed that 2 equiv of 2,4-DNP are released in 42 h for complex **1**, and in 6 h for complex **2**, at 25 °C, which indicates the hydroysis of both the mono- and the diester. On the basis of this information and assuming that the hydrolysis reaction of the 2,4-BDNPP diester leads to the formation of an intermediate (presumable the monoester coordinated to the catalyst), we decided to investigate the catalytic activity of complex **2** in the hydrolysis of the monoester 2,4-DNPP. As can be observed in Figure S7, the determination of the initial rates as a function of substrate concentration reveals saturation kinetics with Michaelis−Menten-like behavior. The kinetic parameters, k_{cat} = 1.42 × 10^{-2} s^{-1} and K_{ass} = 790 mol^{-1}·L reveal that the association constant of the monoester with catalyst **2** is about 5 times greater, while k_{cat} is 27 times lower when compared to those parameters obtained with the correspond-

(48) Carlsson, H.; Haukka, M.; Nordlander, E. *Inorg. Chem.* **2002**, *41*, 4981−4983.
(49) Piszkiewicz, D. *Kinetics of Chemical and Enzyme-Catalized Reactions*; Oxford University Press: New York, 1977, pp 81−106.

Table 4. Kinetics Parameters for the 2,4-BDNPP Hydrolysis Promoted by Complexes **1** and **2** at pH 9.00 and 25 °C

complex	$v_{max} \times 10^8$, mol·L^{-1}·s^{-1}	$K_M \times 10^3$, mol·L^{-1}	$k_{cat} \times 10^3$, s^{-1}	K_{ass},[a] mol^{-1}·L	E,[b] L·mol^{-1}·s^{-1}	f[c] $\times 10^{-3}$
1	5.83	1.19	34.29	840.34	28.82	88.38
2	328.15	5.67	386.06	176.37	68.09	995.00

[a] $K_{ass} = 1/K_M$. [b] $E = k_{cat}/K_M$ (catalytic efficiency). [c] $f = k_{cat}/k_{nc}$ (catalytic factor), where $k_{nc} = 3.88 \times 10^{-7}$ s^{-1} at 25 °C (uncatalyzed reaction constant).[17]

ing 2,4-BDNPP diester (see Table 4). These data allowed us to conclude that distinct nucleophile groups within complex **2** are acting as the catalysts in the hydrolysis of the mono- and diester−phosphate substrates. It is important to note that the spontaneous hydrolysis of the monoester 2,4-DNPP is about 50 times greater than the hydrolysis of the diester 2,4-BDNPP under similar experimental conditions.[17] Here, the opposite is observed, clearly indicating that the hydrolysis reaction of the monoester is occurring through the attack of a poorer nucleophile than that responsible for the catalysis of the diester.

Furthermore, we have also investigated the dependence of the hydrolysis reaction of 2,4-BDNPP on the concentration of complexes **1** and **2**, and the results are shown in Figures S8 and S9, respectively. As can be observed, the kinetic data reveal that for both complexes the rate of hydrolysis is linearly dependent on the concentration of **1** and **2**, and the following second-order rate constants (k_2) were calculated from the slope of the straight lines of k_{obs} versus [complex]: $k_2 = 0.31$ L mol^{-1}·s^{-1} for **1** and $k_2 = 3.35$ L mol^{-1}·s^{-1} for **2**. It is important to note that these second-order rate constants follow the same trend as the k_{cat} values (vide infra), with complex **2** being 10 times more reactive than complex **1**. Interestingly, the second-order rate constant $k_2 = 3.35$ L·mol^{-1}·s^{-1} determined for **2** is smaller but comparable to the catalytic efficiency $k_{cat}/K_M = 11$ L·mol^{-1}·s^{-1} obtained from the kinetic studies of **2** with the monoester under Michaelis−Menten conditions. Therefore, since under experimental conditions of excess complex the release of 2 equiv of 2,4-DNP was always observed, it can be concluded that hydrolysis of the monoester 2,4-DNPP to 2,4-DNP and inorganic phosphate must be the rate determining step of the overall reaction catalyzed by **1** or **2**.

As our main goal is to obtain an effective catalyst, a hydrolysis reaction of 2,4-BDNPP (5.0×10^{-3} mol·L^{-1}) promoted by complexes **1** and **2** (1.0×10^{-5} mol· L^{-1}) at 445 nm, pH 9.00, and 25 °C (Figure S10) was also monitored. These data revealed that both complexes can be considered as efficient catalysts and are able to hydrolyze 22 molecules of substrate in 24 h for complex **1**, and 38 molecules in 6 h for complex **2**.

The isotopic effect was evaluated in order to establish whether the nucleophilic attack on the phosphorus atom was via the terminal hydroxide ion or a general base catalysis. According to Burstyn and co-workers,[50] if $0.80 < (k_H/k_D) < 1.50$, this is indicative that there is no proton transference involved in the reaction limiting step, and suggests an intramolecular nucleophilic attack mechanism.[51] The k_H/k_D ratios obtained for complexes **1** and **2** were 1.16 and 1.10, respectively, which corroborate the presence of a hydrolysis reaction proceeding through an intramolecular mechanism, in which the phosphorus atom undergoes a nucleophilic attack promoted by the coordinated hydroxide ion.

In order to investigate the influence of the acetate ion on the catalytic activity of complexes **1** and **2**, under the experimental conditions employed in the above experiments, the reaction hydrolysis as a function of the acetate concentration was monitored under the same conditions. Figure 6 shows the percentage inhibition of the hydrolysis reaction versus number of acetate equivalents added. As can be observed, addition of 1 or 2 acetate equivalents does not have a strong inhibition influence. Nevertheless, when the acetate concentration equals that of the substrate, this results in a 35% reduction and reaches 55% with the addition of 180 equiv. These results support the finding that the acetate ions are not coordinated to the binuclear complexes at pH 9.00, and they can be considered inhibitors for this reaction when present in high concentrations.

The temperature influence on the hydrolysis reaction was investigated under the same conditions described above for the substrate excess experiments at 20, 25, 30, 35, 40 ± 0.05 °C. Aiming to compare the activation parameters obtained with the values reported for 2,4-BDNPP, the initial rates were converted to k_{obs} by subtracting the dependence of complexes **1** and **2**. As complexes **1** and **2** catalyze the hydrolysis reaction and there is a 100-fold excess of substrate relative to the complexes, the complex concentrations are negligible. The data shown in Table 5 reveal that the rate constants (k_{obs}'s) for the hydrolysis of 2,4-BDNPP promoted by complexes **1** and **2** increase by a factor of 2 under a 10 °C increase in temperature. The activation energies and parameters E_a, $\Delta H^{\ddagger}$, $\Delta S^{\ddagger}$, and $\Delta G^{\ddagger}$ for the reactions catalyzed

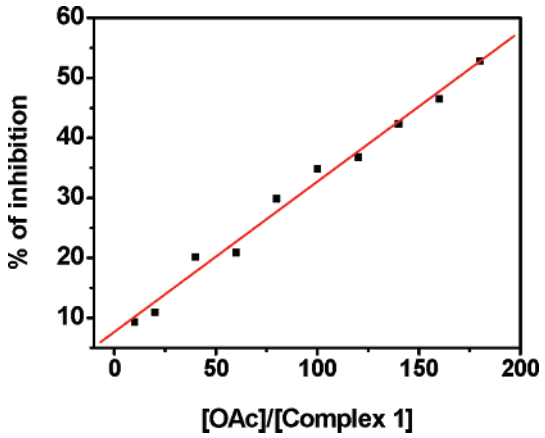

Figure 6. Percentage inhibition of the hydrolysis reaction of the 2,4-BDNPP substrate with acetate catalyzed by complex **1**. Conditions: [1] = 1×10^{-5} mol·L^{-1}, pH = 9.00, H_2O/CH_3CN (50% v/v).

(50) Deal, K. A.; Hengge, A. C.; Burstyn, J. N. *J. Am. Chem. Soc.* **1996**, *118*, 1713−1718.
(51) Gold, V. *Adv. Phys. Org. Chem.* Academic Press: New York, 1967.

Table 5. Effect of Temperature on the Hydrolysis Reaction Rate of 2,4-BDNPP

	$k_{obs} \times 10^3$, s^{-1}	
T (K)	complex **1**	complex **2**
293	1.34 ± 0.13	33.99 ± 0.61
298	2.31 ± 0.11	46.38 ± 0.51
303	3.19 ± 0.20	62.99 ± 0.92
308	4.85 ± 0.19	87.50 ± 0.97
313	7.04 ± 0.22	117.46 ± 4.05

Table 6. Activation Parameters for the Hydrolysis of 2,4-BDNPP

	E_a, kJ·mol^{-1}	$\Delta H^{\ddagger}$, kJ·mol^{-1}	$\Delta S^{\ddagger}$, J·mol^{-1}·K^{-1}	$\Delta G^{\ddagger}$,[a] kJ·mol^{-1}
complex **1**	60	57	−103	88
complex **2**	48	45	−119	81
HO^{-}[b]		80	−107	111

[a] $\Delta G^{\ddagger} = \Delta H^{\ddagger} - T\Delta S^{\ddagger}$, at 25 °C. [b] General basic catalysis.[53]

by complexes **1** and **2** were obtained through the Eyring[52] and the Arrhenius equations.[52] Figures 7 and S11 show the linearization of the observed rate constants (k_{obs}'s) for the reactions catalyzed by complexes **2** and **1**, respectively. Unfortunately, there are no activation parameters reported for the hydrolysis of 2,4-BDNPP in the presence of metal complexes, and no comparisons can thus be made. Table 6 gives the activation thermodynamics parameters for the hydrolysis of this substrate catalyzed by complexes **1** and **2**, and those obtained for the uncatalyzed reaction.[53]

As observed, the data indicate that, in the presence of complexes **1** and **2**, the free energy of activation decreases, as expected for compounds acting as catalysts. It is worth noting that the reaction promoted by complex **2** is favored. In both cases, $\Delta S^{\ddagger} < 0$ which indicates that an organization of the reactive species occurs in the transition states. In parallel, $\Delta H^{\ddagger} > 0$ which reflects bond making in the activated complex. The activation energy for the reaction carried out in the presence of complex **2** is lower than that obtained for complex **1**, and is in agreement with the observed reaction rates. Considering the data presented in Table 6, one can conclude that the 2,4-BDNPP hydrolysis promoted by complexes **1** and **2** occurs through a similar mechanism.

Mechanism Proposal. Some of the evidence for the proposed mechanism is based on the characterization of complexes **1** and **2**. On the basis of the crystallographic data, magnetochemistry, and electronic spectra in the solid state and solution, and conductivities of complexes **1** and **2**, the presence of species **a** is supported in acetonitrile solution (Scheme 1). In view of this, the potentiometric titrations were carried out aiming to assess the lability of the acetate bridges, and two titratable protons were determined. Thus, species **b** is proposed to be the active species in the hydrolysis of the diester 2,4-BDNPP under the experimental conditions employed in the kinetics experiments. Usually, octahedral Ni^{II} complexes with monodentate ligands involved in ligand substitution reactions have a preference for dissociative

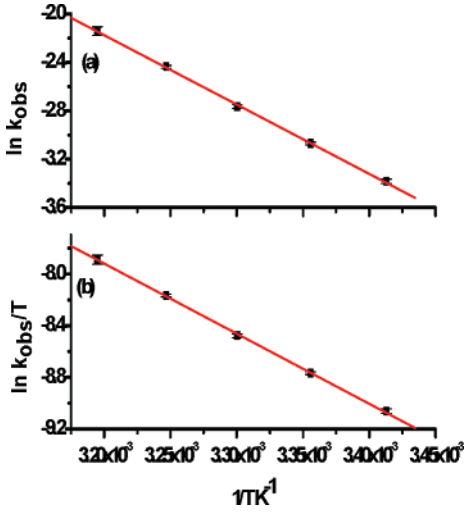

Figure 7. Linearizations of the observed rate constants for the hydrolysis of 2,4-BDNPP (1.0×10^{-3} mol·L^{-1}) promoted by complex **2** (1.0×10^{-5} mol·L^{-1}) at pH 9.00 as a function of temperature: (a) Arrhenius equation and (b) Eyring equation.

mechanisms with the formation of a square pyramid intermediate (ML_5).[54] In this system (Scheme 1), intermediate **c** would be favored because of the presence of the polydentate ligand which occupies four of the coordination positions in the Ni1 center, and of the exogenous μ-hydroxo bridge.

During the reactivity studies, the following conditions were always rigorously maintained under control: the concentrations of complexes **1** and **2**, pH, ionic strength, temperature, and substrate excess. In addition, both systems (for complexes **1** and **2**) presented Michaelis−Menten type kinetics. Thus, it is proposed that the coordination of the substrate occurs through the replacement of a water molecule. In this way, the substrate is oriented in a *cis* position with respect to the hydroxide, and the nucleophilic attack takes place on the phosphorus atom. The possibility for a general basic catalysis decreased in view of the results obtained in the studies on the isotopic deuterium effects, which revealed the involvement of the complexes in the intramolecular attack prior to the diester hydrolysis. In light of these data, the formation of species **d** is proposed (Scheme 1).

In general, intramolecular nucleophilic attack has been associated with high reaction rates because of the increase in the system order.[55] The activation parameters obtained indicate bond making and a decrease in the disorder in the transition state, which is consistent with an intramolecular nucleophilic attack which leads to the formation of the hydrolysis product 2,4-DNP.

According to Bunton and co-workers,[17] the spontaneous hydrolysis of 2,4-BDNPP occurs through the breaking of the oxygen−phosphorus bond, generating the 2,4-DNP and

(52) Wilkins, R. G. *Kinetics and Mechanism of Reactions of Transition Metal Complexes*, 2nd ed.; VCH: Weinheim, 1991.
(53) Kirby, A. J.; Younas, M. *J. Chem. Soc. B* **1970**, 510−513.
(54) Atkins, P. W.; Shriver, D. F. *Inorganic Chemistry*, 3rd ed.; Oxford University Press: New York, 1999.
(55) Menger, F. M. *Acc. Chem. Res.* **1985**, *18*, 128−134.
(56) Young, M. J.; Wahnon, D.; Hynes, R. C.; Chin, J. *J. Am. Chem. Soc.* **1995**, *117*, 9441−9447.
(57) Chin, J.; Zou, X. *J. Am. Chem. Soc.* **1988**, *110*, 223−225.
(58) Duboc-Toia, C.; Megane, S.; Vincent, J.-M.; Averbuch-Pouchot, M. T.; Fontecave, M. *Inorg. Chem.* **1997**, *36*, 6148−6149.

Scheme 1. Proposed Mechanism for the Hydrolysis of 2,4-BDNPP Promoted by Complexes **1** and **2**

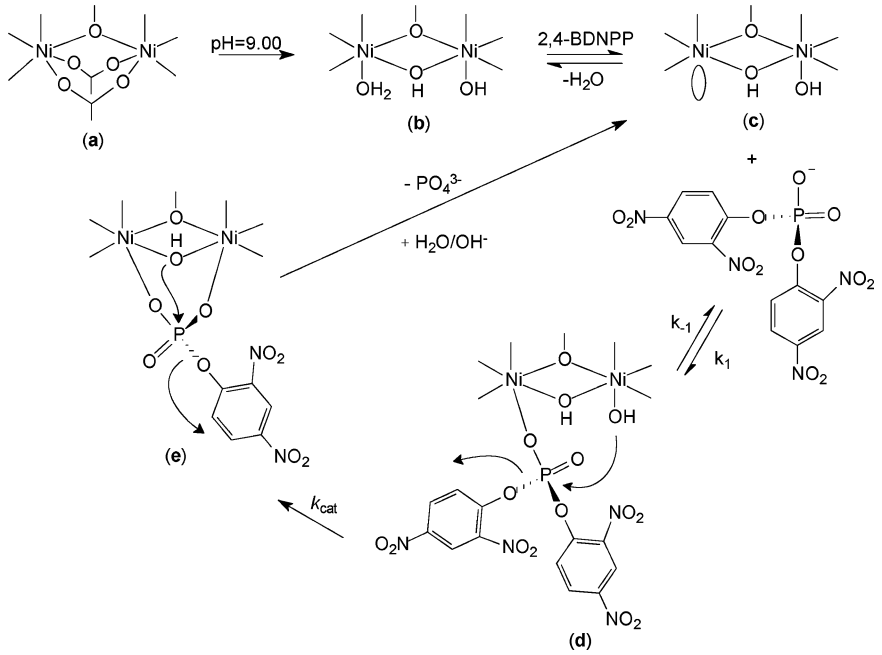

inorganic phosphate. The reaction takes place in two steps according to eq 4, with $k' > k$.

$$(ArO)_2PO_2^- \xrightarrow{k} ArO^- + ArOPO_3^{2-} \xrightarrow{k'} ArO^- + PO_4^{3-} \quad (4)$$

Since stoichiometric reactions between complexes **1** (and **2**) and 2,4-BDNPP released 2 equiv of 2,4-DNP, species **e** is proposed, in which the monoester 2,4-DNPP bridges the two Ni^{II} centers through the μ-phosphate group. In addition, kinetic studies of **2** with the 2,4-DNPP monoester reveal a $K_{ass} = 790\ mol^{-1}\ L$ which is about 5 times greater than the value found for the 2,4-BDNPP diester under Michaelis−Menten experimental conditions. With the presence of such a phosphate bridge, the monoester 2,4-DNPP becomes activated by the two nickel centers, and in principle, an intramolecular nucleophilic attack of the μ-hydroxide would be responsible for the hydrolysis of the bound monoester (species **d**). This is because the bridge approximates the μ-hydroxide group to the phosphorus center facilitating the intramolecular nucleophilic attack and the release of the other 2,4-DNP. On this basis and considering the results recently obtained by Neves et al.[59] in which it has been demonstrated that in the [(OH)Fe(III)(μ-OH)Zn(II)] complex the μ-hydroxo is a significantly poorer nucleophile than the terminally Fe(III)-bound OH^- group, it is suggested that the diester 2,4-BDNPP reacts faster than the monoester 2,4-DNPP. Therefore, the hydrolysis reaction of 2,4-DNPP is the rate-limiting step of the reaction.

All attempts to isolate species **e** using 2,4-BDNPP, or the less activated analogous bis(4-nitrophenyl)phosphate, were unsuccessful. Finally, under the excess of substrate conditions at pH 9.00, species **c** is regenerated, and the catalytic cycle is completed.

Some of the studies reported in the literature[6,7,10−12,56−58] used 2,4-BDNPP as the substrate. The most active compound to date is a heterobinuclear $Fe^{III}Cu^{II}$ reported by Lanznaster and co-workers,[13] which speeds up the reaction by a factor of 10^4. Here we present, to the best of our knowledge, the most effective complexes (**1** and **2**) reported to date, speeding up the hydrolysis reaction rate by factors of 8.8×10^4 and 9.95×10^5, respectively, compared to the uncatalyzed basic hydrolysis of 2,4-BDNPP. Thus, as the most effective compounds, complexes **1** and **2** are undoubtedly highly efficient functional models of the phosphohydrolases.

Conclusions

In summary, we have synthesized and characterized a novel structural model complex (**2**) of ureases, which is composed of two Ni^{II} centers coordinated to a new unsymmetrical N,O-donor ligand and has a metal−metal distance (3.486(1) Å) similar to the 3.5 Å present in the bacterial urease from *Klebsiella aerogenes*.[33] Complexes **1** and **2** possess excellent catalytic ability to hydrolyze 2,4-BDNPP presenting catalytic activities 8.8×10^4 and 9.95×10^5 times faster, respectively, in relation to the uncatalyzed reaction. On the basis of structural, kinetic, thermodynamic, and activation parameter data, a catalytic mechanism cycle is proposed for the hydrolysis of 2,4-BDNPP promoted by complexes **1** and **2**. This mechanism includes intramolecular nucleophilic attack involving two steps: (i) an attack of the terminal hydroxide coordinated to a Ni^{II} center on the phosphorus atom bound to the other Ni^{II} center, followed by a slower step consisting of (ii) an attack of the hydroxo bridge on the phosphorus of the phosphate bridge. This mechanistic proposal is somewhat pioneering in bioinorganic chemistry in the sense that we have a model system with inherent catalytic competence in both monoesterase and diesterase hydrolysis, a capability that has been recently

(59) Neves, A.; Lanznaster, M.; Bortoluzzi, A. J.; Peralta, R. A.; Casellato, A.; Castellano, E. E.; Herrald, P.; Riley, M. J.; Schenk, G. *J. Am. Chem. Soc.* **2007**, *129*, 7486−7487.

demonstrated for pig purple acid phosphatase.[60] Furthermore, a mechanism in which the μ-OH^- serves as the nucleophile attacking the polarized carbonyl moiety of a bridging amide group has also been proposed for urease.[33,61]

(60) Cox, R. S.; Schenk, G.; Mitic, N.; Gahan, L. R.; Hengge, A. *J. Am. Chem. Soc.* **2007**, *129*, 9550−9551.
(61) Benini, S.; Rypniewski, W. P.; Wilson, K. S.; Miletti, S.; Ciurli, S.; Mangani, S. *Structure* **1999**, *7*, 205−216.

Acknowledgment. The authors are grateful for grants provided by CNPq, FINEP, Capes, and Pronex (Brazil) and DLR (Germany) for support of this research. We are grateful to Dr. Juraj Pelikan for magnetic measurements of complex **2**.

Supporting Information Available: Figures S1−S11 in PDF format. This material is also available free of charge via Internet at http://pubs.acs.org.

IC702132T